# Electrocatalytic Activity of layered oxides $SrLaAl_{1/2}M_{1/2}O_4$ (M = Mn, Fe, Co) for Hydrogen- and Oxygen-Evolution Reactions

Md. Sofiul Alom[1], Farshid Ramezanipour[1,*]

[1]Department of Chemistry, University of Louisville, Louisville, KY 40292, USA

*Corresponding author. Email: farshid.ramezanipour@louisville.edu, Phone: +1(502) 852-7061

ORCID: 0000-0003-4176-1386

## ABSTRACT

A series of quasi-2D oxides, with formula $SrLaAl_{1/2}M_{1/2}O_4$ (M = Mn, Fe, Co), have been synthesized and their electrocatalytic activity has been investigated for both half reactions of water splitting, namely oxygen evolution reaction (OER) and hydrogen evolution reaction (HER). These layered oxides consist of octahedrally coordinated Al/M metals, where the octahedra are separated by alkaline earth/rare earth cations. Among the synthesized materials, $SrLaAl_{1/2}Co_{1/2}O_4$ shows the best performance, evident from considerably lower overpotentials for OER and HER, as well as faster reaction kinetics, evaluated by the Tafel method. The improved performance of $SrLaAl_{1/2}Co_{1/2}O_4$ is explained in terms of a combination of factors, including the greater bond covalency due to the higher electronegativity of Co than Mn and Fe, as well as the favorable electronic configuration of trivalent cobalt. Importantly, the electrical conductivity studies indicate a correlation between charge transport and the electrocatalytic activity, where the most active catalyst also shows the highest electrical conductivity.

Keywords: Oxides; Electrocatalytic activity; OER; HER

## INTRODUCTION

Finding sustainable sources of energy will be one of the most challenging issues of the next century. It is urgent to access clean energy sources, given the growing global energy demand and environmental concerns. Renewable sources, such as solar and wind, are excellent alternatives to fossil fuels, but their intermittent nature limits their application.[1, 2] Hydrogen is widely considered a clean and renewable energy source to replace carbon emitting fossil fuels owing to its environmental compatibility and high specific energy. Electrochemical water splitting is a promising approach for sustainable hydrogen production.[3, 4] The process of electrochemical water splitting occurs via two half-reactions, namely oxygen evolution reaction (OER) and hydrogen evolution reaction (HER). Theoretically, a cell potential of 1.23 V (vs. reversible hydrogen electrode) is required to drive this process, but in practice, it requires a considerable overpotential to overcome the activation energy barrier, especially for OER.[5]

Precious metal catalysts, such as $IrO_2$[6] and $RuO_2$[7] for OER, and Pt/C[8, 9] for HER have been utilized to facilitate these processes by reducing the overpotentials. However, the high cost of these catalysts has motivated the search for more economical alternatives.[10, 11] Perovskite related oxides can be excellent candidates for this application due to their stability and compositional and structural variety. Some of the catalysts in this family have shown great promise, especially for OER, such as $Ba_{0.5}Sr_{0.5}Co_{0.8}Fe_{0.2}O_{3-\delta}$ (BSCF).[12] Several perovskite-related electrocatalysts have also been reported by our group.[13-20] A related class of oxides are those having the general formula $A_2BO_4$, where A is often an alkaline earth metal or a lanthanide and B is usually a transition metal (Figure 1). This family of oxides are structural analogues of the fluoride $K_2NiF_4$. Therefore, they are often referred to as $K_2NiF_4$-type oxides. These oxides have been studied in various fields, such as solid oxide fuel cells (SOFC),[21-23] superconductivity,[24, 25] spintronics,[26, 27] magnetism,[28, 29] and

pseudocapacitance[30]. However, few reports are found about the electrocatalytic activity of this class of oxides for water-splitting.[18, 31, 32]

In this work, the enhancement of the electrocatalytic properties as a function of B site cation in $SrLaAl_{1/2}Mn_{1/2}O_4$, $SrLaAl_{1/2}Fe_{1/2}O_4$, and $SrLaAl_{1/2}Co_{1/2}O_4$ is investigated. Among them, $SrLaAl_{1/2}Co_{1/2}O_4$ has been reported and the influence of chemical bonding on its spin states has been studied.[33] However, its electrocatalytic properties have remained unexplored. In the present work, we have synthesized this material, along with two new compounds, and have demonstrated the systematic changes of their electrocatalytic performance for both half-reactions of water-splitting.

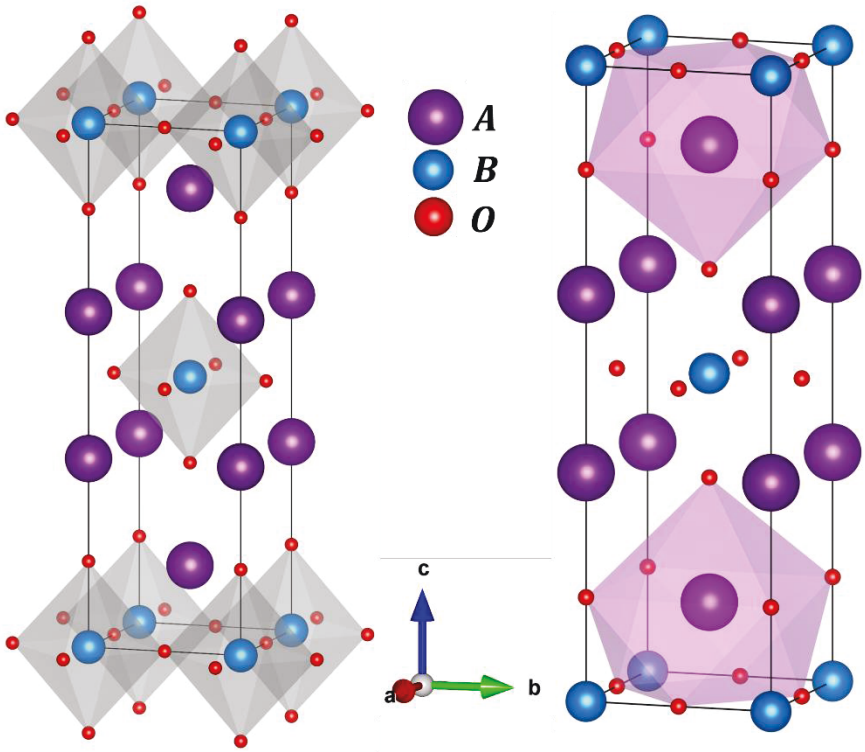


**Figure 1.** Crystal structure of $SrLaAl_{1/2}M_{1/2}O_4$ (M = Mn, Fe, Co), showing (a) the octahedral coordination geometry of M/Al (blue spheres), and (b) the coordination of Sr/La (purple spheres). In part (b), only two polyhedra are shown for clarity.

## EXPERIMENTAL

The materials $SrLaAl_{1/2}Mn_{1/2}O_4$, $SrLaAl_{1/2}Fe_{1/2}O_4$, and $SrLaAl_{1/2}Co_{1/2}O_4$ were synthesized by solid state method. Stoichiometric amounts of $SrCO_3$, $La_2O_3$, $Al_2O_3$, $Mn_2O_3$, $Fe_2O_3$, and $Co_3O_4$ were mixed thoroughly by agate mortar and pestle, and pressed into pellets. These pellets were calcined at 1250 °C for 96 hours with intermediate grinding and refiring. The heating and cooling rates were set to be 100 °C per hour. $SrLaAl_{1/2}Fe_{1/2}O_4$ and $SrLaAl_{1/2}Co_{1/2}O_4$ samples were heated in air, whereas $SrLaAl_{1/2}Mn_{1/2}O_4$ was heated under argon to obtain a pure phase. The air synthesis for this compound led to an impure product. In addition, for the purpose of comparison, the synthesis of the Al-only compound, $SrLaAlO_4$, was attempted under the same conditions in air. However, it consistently led to impure products. Whereas the three compounds containing transition metals could all be obtained as pure single phase products. The crystal structures of these compounds were determined by high resolution powder X-ray diffraction (PXRD) using Cu Kα1 radiation with a wavelength of $\lambda = 1.540556$ Å. GSAS software[34] and EXPEGUI interface[35] were used for Rietveld refinements. Oxygen content was determined by iodometric titration described elsewhere.[36, 37] Electrical conductivity measurements were done on sintered pellets by a 4-point probe direct-current (DC) method. Electrocatalytic activities were studied on an electrochemical workstation with a standard three electrode glass cell system using a rotating disk electrode at 1600 rpm. The reference electrodes were a commercial Ag/AgCl electrode in 1 M KCl (CH instruments, Inc.) and an Ag/AgCl electrode in saturated KCl (Pine Research Instrumentation Inc.) for the OER and HER experiments, respectively. The counter electrode for OER was a platinum electrode. Whereas, for HER, a carbon electrode was used to avoid the possible dissolution of the platinum electrode in acidic condition and its contribution to the HER.[38] A glassy carbon (GC) disk electrode (geometrical surface area 0.196 $cm^2$) loaded with the catalyst ink was used as the working electrode

for both HER and OER. The catalyst ink was prepared by mixing 35 mg of the catalyst powder, 7 mg of carbon black (Fuel Cell Store) and 40 µL of Nafion D-521 solution (Alfa Aesar, 5% w/w in water and 1-propanol) and 7 mL of Tetrahydrofuran (Alfa Aesar, 99%). The mixture was sonicated for 10 minutes to make it homogeneous. The added carbon black helps the catalysis process by enhancing the electrical conductivity and maximizing the utilization of the catalyst.[39-41] 20 µL of the catalyst ink was dropcasted on the GC electrode, in 10 µL increments and an interval of one minute, and was dried for 24 hours in air. Cyclic voltammetry (CV) data for OER and HER were recorded at a scan rate of 10 $mVs^{-1}$ and 20 $mVs^{-1}$, respectively. Chronopotentiometry was employed to study the stability of the catalyst in different electrolytes. Chronopotentiometry under OER conditions was done using a two-electrode setup on nickel foam electrodes to avoid the corrosion of the glassy carbon electrode upon prolonged exposure to the oxidative conditions. For this purpose, two square pieces of nickel foam with dimensions of 1 $cm^2$ were each loaded with 100 µL of catalyst ink in 10 µL increments, followed by overnight drying. The nickel foam electrodes were separated by a glass fiber filter paper, and were connected to the potentiostat through gold leads connected to gold wires. The cell was soaked into the electrolyte solution for 12 hours before the experiment.

## RESULTS ND DISCUSSION

### Crystal Structure

The X-ray diffraction patterns of $SrLaAl_{1/2}M_{1/2}O_4$ (M = Mn, Fe, Co) are shown in Figure 2. All three compounds have tetragonal *I*4/*mmm* space group, consistent with a previous structural report for the Co compound.[33] The refined structural parameters are listed in Tables 1-3.

**Table 1.** Refined structural parameters for $SrLaAl_{1/2}Co_{1/2}O_4$ using powder X-ray diffraction data. Space group: *I4/mmm*, *a* = 3.78562(2) Å, *c* = 12.5157 (1) Å Rp = 0.0345, wRp = 0.0462

| Atom | Multiplicity | Occupancy | x | y | z | $U_{iso}$ |
|---|---|---|---|---|---|---|
| Sr | 4 | ½ | 0 | 0 | 0.3599(1) | 0.0276(5) |
| La | 4 | ½ | 0 | 0 | 0.3599(1) | 0.0276(5) |
| Co | 2 | ½ | 0 | 0 | 0 | 0.023(2) |
| Al | 2 | ½ | 0 | 0 | 0 | 0.020(2) |
| O1 | 4 | 1 | 0 | 0.5 | 0 | 0.030(4) |
| O2 | 4 | 1 | 0 | 0 | 0.1638(9) | 0.023(3) |

**Table 2.** Refined structural parameters for $SrLaAl_{1/2}Fe_{1/2}O_4$ using powder X-ray diffraction data. Space group: *I4/mmm*, *a* = 3.8180(1) Å, *c* = 12.7035 (4) Å Rp = 0.0359, wRp = 0.0471

| Atom | Multiplicity | Occupancy | x | y | z | $U_{iso}$ |
|---|---|---|---|---|---|---|
| Sr | 4 | ½ | 0 | 0 | 0.3589(1) | 0.0129(5) |
| La | 4 | ½ | 0 | 0 | 0.3589(1) | 0.0129(5) |
| Fe | 2 | ½ | 0 | 0 | 0 | 0.011(2) |
| Al | 2 | ½ | 0 | 0 | 0 | 0.011(2) |
| O1 | 4 | 1 | 0 | 0.5 | 0 | 0.005(4) |
| O2 | 4 | 1 | 0 | 0 | 0.170(1) | 0.028(4) |

**Table 3.** Refined structural parameters for $SrLaAl_{1/2}Mn_{1/2}O_4$ using powder X-ray diffraction data. Space group: *I4/mmm*, *a* = 3.7755(2) Å, *c* = 12.8873 (8) Å Rp = 0.0474, wRp = 0.0658

| Atom | Multiplicity | Occupancy | x | y | z | $U_{iso}$ |
|---|---|---|---|---|---|---|
| Sr | 4 | ½ | 0 | 0 | 0.35735(8) | 0.0105(5) |
| La | 4 | ½ | 0 | 0 | 0.35735(8) | 0.0105(5) |
| Mn | 2 | ½ | 0 | 0 | 0 | 0.002(1) |
| Al | 2 | ½ | 0 | 0 | 0 | 0.002(1) |
| O1 | 4 | 1 | 0 | 0.5 | 0 | 0.045(3) |
| O2 | 4 | 1 | 0 | 0 | 0.1656(5) | 0.022(2) |

In these $A_2BO_4$ oxides (A = Sr/La and B = $Al_{1/2}Mn_{1/2}$, $Al_{1/2}Fe_{1/2}$, $Al_{1/2}Co_{1/2}$), the $BO_6$ octahedra are distorted. The B-O distances in the basal plane (*ab* plane) are shorter than the apical B-O bonds, as listed in Table 4. Each $BO_6$ octahedron is connected to four neighboring $BO_6$ octahedra in the *ab* plane through common O atoms. The A site cation is surrounded by nine oxygen atoms, as shown in Figure 1b.

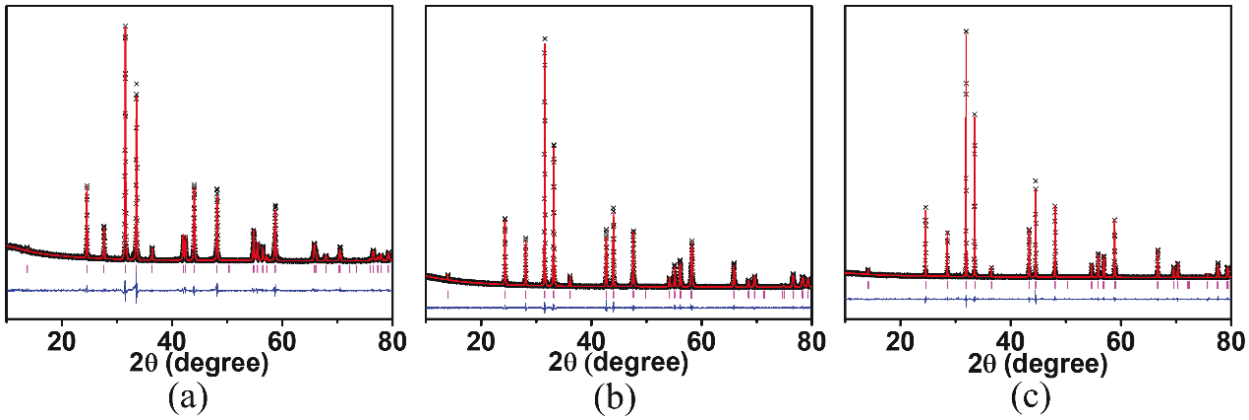


**Figure 2.** Rietveld refinement profiles for powder X-ray diffraction data of (a) $SrLaMn_{0.5}Al_{0.5}O_4$, (b) $SrLaFe_{0.5}Al_{0.5}O_4$ and (c) $SrLaCo_{0.5}Al_{0.5}O_4$. The black crosses, the solid red line, the vertical pink lines and lower blue line represent the experimental data, calculated model, Bragg peak positions and difference plot, respectively.

**Table 4.** Bond lengths in $BO_6$ octahedra.

| Sample | Apical B-O length (Å) | Equatorial B-O length (Å) |
|---|---|---|
| $SrLaAl_{1/2}Co_{1/2}O_4$ | 2.050(1) | 1.89281(1) |
| $SrLaAl_{1/2}Fe_{1/2}O_4$ | 2.162(2) | 1.90899(6) |
| $SrLaAl_{1/2}Mn_{1/2}O_4$ | 2.134(6) | 1.8878(1) |

Similar to the perovskite structure, the stability of oxides with $K_2NiF_4$ structure can be expressed in terms of a tolerance factor, t, as follows:[42]

$$t = \frac{r_A + r_o}{\sqrt{2}(r_B + r_o)}$$

Where, $r_A$, $r_B$ and $r_O$ are ionic radii of the A site cation, B site cation and oxygen, respectively. If there are multiple atoms at A or B site, then the average ionic radius is used to calculate the tolerance factor. The $A_2BO_4$ oxides usually crystallize either in tetragonal or orthorhombic structure. The range of tolerance factor for tetragonal structure is $0.99 \geq t \geq 0.88$ and for orthorhombic structure $0.88 > t \geq 0.865$.[43-45]

While the $r_B$ values in the above formula depend on the spin state of the transition metal, some ions such as $Fe^{3+}$ are commonly found in high-spin state in ambient conditions.[46] As an example of the utilization of this formula, using Shannon's ionic radii ($r_{Sr^{2+}} = 1.31$ Å and $r_{La^{3+}} = 1.216$ Å for CN = 9; $r_{Fe^{3+}} = 0.645$ Å for CN = 6, HS),[47] the calculated tolerance factor for the Fe-containing material is found to be 0.946, which falls well within the range expected for tetragonal symmetry.

Iodometric titrations confirmed the oxygen stoichiometry in these materials to be 4 oxygen per formula unit. This is consistent with trivalent state of transition metals in these materials. As will be discussed later, $SrLaAl_{1/2}Co_{1/2}O_4$ shows the best electrocatalytic activity among the three compounds. Therefore, X-ray photoelectron spectroscopy was used to confirm the oxidation state of the transition metal in this compound. As shown in Figure 3, the $2p_{3/2}$ peak for cobalt appears just above 780 eV, along with a satellite peak at about 10 eV higher. This is consistent with $Co^{3+}$,[48] as expected for $SrLaAl_{1/2}Co_{1/2}O_4$.

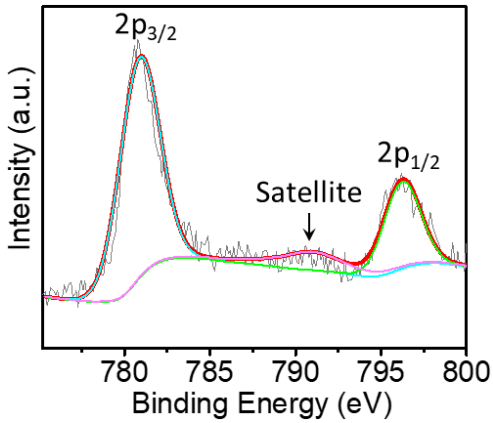


**Figure 3.** X-ray photoelectron spectroscopy data for $SrLaAl_{1/2}Co_{1/2}O_4$, showing the Co spectrum.

**Hydrogen Evolution Reaction (HER)**

We have investigated the utilization of these materials as electrocatalysts for HER. The generally accepted mechanism of HER in both acidic and alkaline media is a two-step process which involves two electron transfers.[49-51] In the first step, the Volmer reaction, a hydronium ion ($H_3O^+$) in acidic conditions is reduced on the surface of the catalyst to form an adsorbed hydrogen (M-H*) intermediate. The second step is either electrochemical interaction of the adsorbed hydrogen with another $H_3O^+$ ion to produce molecular $H_2$, known as Heyrovsky reaction, or the combination of two adsorbed hydrogen atoms to give $H_2$, known as Tafel reaction.

(1) Volmer: $M + H_3O^+ + e^- \rightarrow M\text{-}H + H_2O$

(2) Heyrovsky: $H_3O^+ + M\text{-}H + e^- \rightarrow H_2\uparrow + H_2O + M$

or

(2) Tafel: $2M\text{-}H \rightarrow H_2\uparrow + 2M$

The HER in basic medium follows a similar mechanism, except the proton source is $H_2O$ instead of $H_3O^+$. [51]

(1) Volmer: $M + H_2O + e^- \rightarrow M\text{-}H + OH^-$

(2) Heyrovsky: $H_2O + M\text{-}H + e^- \rightarrow H_2\uparrow + OH^- + M$

or

(2) Tafel: $2M\text{-}H \rightarrow H_2\uparrow + 2M$

HER is more favorable in acidic environment than in basic medium due to the presence of a high concentration of protons.[52] In alkaline medium, proton comes from the dissociation of water, which introduces an additional energy barrier. In case of acidic medium, the source of proton is the $H_3O^+$ ion which gives up proton easily. Therefore, the HER process is expected to be more facile in acidic medium.[4]

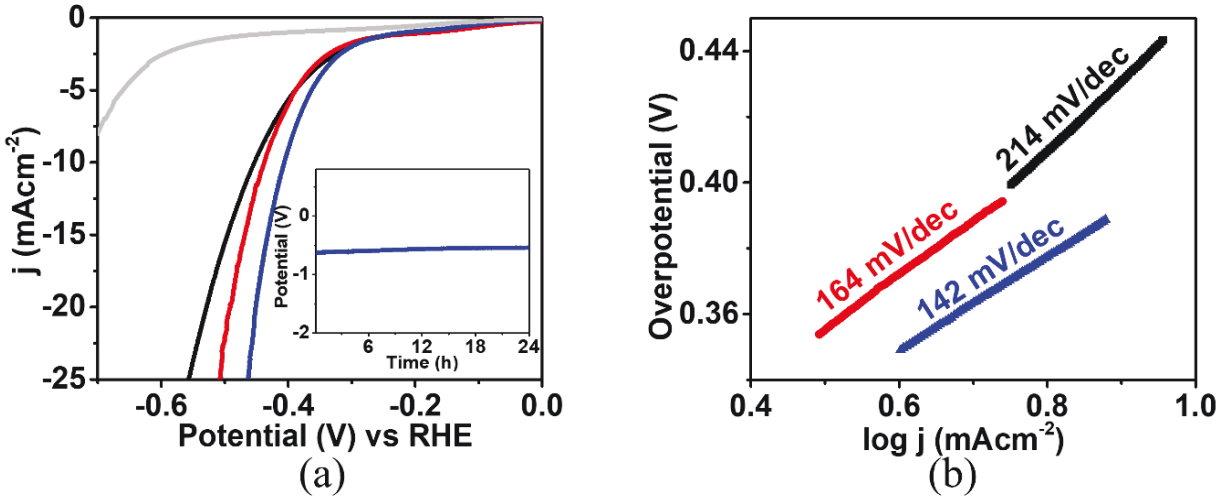


**Figure 4.** (a) Polarization curve for HER activities of $SrLaAlO_4$ (gray, impure), $SrLaAl_{1/2}Mn_{1/2}O_4$ (black), $SrLaAl_{1/2}Fe_{1/2}O_4$ (red), and $SrLaAl_{1/2}Co_{1/2}O_4$ (blue) in 0.5 M $H_2SO_4$. The inset shows chronopotentiometry data for the best performing catalyst, $SrLaAl_{1/2}Co_{1/2}O_4$, at 10 $mAcm^{-2}$. (b) Tafel plot and Tafel slopes for the three materials.

In this work, the HER activity of $SrLaAl_{1/2}M_{1/2}O_4$ (M = Mn, Fe, Co) was studied in both basic and acidic conditions. Experiments in a basic medium, 1 M KOH, led to negligible HER activities, whereas those in acidic conditions, 0.5 M $H_2SO_4$, showed significantly greater performance. The overpotential at -10 $mAcm^{-2}$ ($\eta_{10}$), a current density related to solar fuel synthesis, is a common metric for comparison of the HER activities. In this work, the overpotential values in 0.5 M $H_2SO_4$ are $\eta_{10}$ = 453, 437, and 406 mV, for $SrLaAl_{1/2}Mn_{1/2}O_4$, $SrLaAl_{1/2}Fe_{1/2}O_4$, and $SrLaAl_{1/2}Co_{1/2}O_4$, respectively (Figure 4a). In addition, the $SrLaAlO_4$ sample (impure) was tested, showing negligible activity (grey plot in Figure 4a). The HER overpotentials of these catalysts are not as good as those reported for Pt/C (less than 100 mV)[15, 53-55] and some oxides such as $SrCa_2GaMn_2O_8$ ($\eta_{10}$ = 315 mv)[15] and $CaSrFeMnO_{6-\delta}$ ($\eta_{10}$ = 310 mV).[16] However, the activity of $SrLaAl_{1/2}Co_{1/2}O_4$ is better than those of some other reported catalysts, such as $Sr_2LaCoMnO_7$ ($\eta_{10}$ = 612 mV),[19] $WO_3$ ($\eta_{10}$ = 637 mV),[56] and $LaFeO_3$ ($\eta_{10}$ = 490 mV).[57]

We have also evaluated the relative kinetics of the HER for different catalysts. Faster reaction kinetics is often associated with higher electrocatalytic activity. To study the OER kinetics, Tafel slope is generally used, which can be obtained using Tafel equation:[58, 59]

$$\eta = a + b \log j$$

where, overpotential and current density are denoted by $\eta$ and $j$, respectively. The slope of the Tafel plot, $\eta$ vs log $j$, is influenced by mass and electron transfer,[60, 61] and indicates the reaction kinetics. Smaller slope corresponds to faster reaction, which indicates a small positive shift in potential beyond the onset potential is required to produce a large amount of current.[18]

As shown in Figure 4b, the Tafel slopes of $SrLaAl_{1/2}Mn_{1/2}O_4$, $SrLaAl_{1/2}Fe_{1/2}O_4$, and $SrLaAl_{1/2}Co_{1/2}O_4$ are 214 $mVdec^{-1}$, 164 $mVdec^{-1}$, and 142 $mVdec^{-1}$, respectively. The latter compound shows the lowest Tafel slope and fastest reaction kinetics in the series. The value of Tafel slope can also indicate the rate determining step of the reaction.[62] The expected Tafel slope values are 120 $mVdec^{-1}$, 40 $mVdec^{-1}$ or 30 $mVdec^{-1}$, if the rate determining steps are Volmer, Heyrovsky or Tafel reaction, respectively.[16, 18, 63] However, other values of Tafel slope are also possible if more than one of the three steps dictate the rate of the reaction. For example, the Tafel slope is found to be 166 $mVdec^{-1}$ for $Mo_2C$ film, which is attributed to having two or three rate determining steps.[63] Similarly, larger Tafel slopes indicating mixed reaction mechanism have been reported for Co/NBC,[64] P-doped $NiMoO_4$,[65] $MoS_2$/graphene,[66] and surface-functionalized $MoS_2$ nanosheets.[67]

Chronopotentiometry experiment for the best performing material, $SrLaCo_{0.5}Al_{0.5}O_4$ shows a stable HER activity for at least 24 hours, as shown in the inset of Figure 4a. However, X-ray diffraction shows that this catalyst loses its structural integrity if the HER is done over 1000 cycles in acidic medium.

**Oxygen Evolution Reaction (OER)**

OER in alkaline medium is a four-electron transfer process, as given by the following steps.[19, 68-70] In the first step, a hydroxide ion is adsorbed on the catalyst, accompanied by a 1-electron oxidation to give M-OH. In the second step, another hydroxide ion approaches M-OH to remove a proton and form M-O and water, along with another 1-electron oxidation. In the third step, M-O is converted into a hydroperoxide intermediate M-OOH by nucleophilic attack of a hydroxide ion coupled with a 1-electron oxidation. Finally, M-OOH reacts with another hydroxide ion to release $O_2$, water and an electron. Alternatively, a combination of two M-O intermediates could directly yield $O_2$ and M.[68, 70]

$$M + OH^- \rightarrow M\text{-}OH + e^-$$

$$M\text{-}OH + OH^- \rightarrow M\text{-}O + H_2O + e^-$$

$$M\text{-}O + OH^- \rightarrow M\text{-}OOH + e^-$$

$$M\text{-}OOH + OH^- \rightarrow M + O_2\uparrow + H_2O + e^-$$

or

$$M\text{-}O + M\text{-}O \rightarrow 2M + O_2\uparrow$$

Cyclic voltammetry (CV) is used to study the electrocatalytic activities of OER catalysts. Figure 5a shows the OER polarization curves of $SrLaAl_{1/2}Mn_{1/2}O_4$, $SrLaAl_{1/2}Fe_{1/2}O_4$, and $SrLaAl_{1/2}Co_{1/2}O_4$ in 0.1 M KOH. This condition gave the best results among the acidic and basic conditions, which were attempted. One of the parameters used for comparison of the performance of different OER catalysts is the onset potential, i.e., the potential at which faradic reaction starts. This can be deduced from the CV, by finding the potential at which the sharp rise in current begins. However, as some researchers have pointed out, this may lead to some variation in interpretation of the data by different observers, who may assign different onset potentials to the same data.[71] It

has been suggested that the onset potential is taken as the potential at a low current response, as small as 0.05 $mAcm^{-2}$.[71] We note that this approach may also lead to some difficulty in comparison of the data, since different researchers may choose a different current response for determination of the onset potential. In this work, the onset potential is taken as the potential at a low current density of 0.1 $mAcm^{-2}$, which gives 1.46, 1.52 and 1.34 V for $SrLaAl_{1/2}Mn_{1/2}O_4$, $SrLaAl_{1/2}Fe_{1/2}O_4$, and $SrLaAl_{1/2}Co_{1/2}O_4$, respectively. The lower onset potential of the latter material compared to the others indicates that the catalytic reaction starts earlier, indicating a better OER activity.

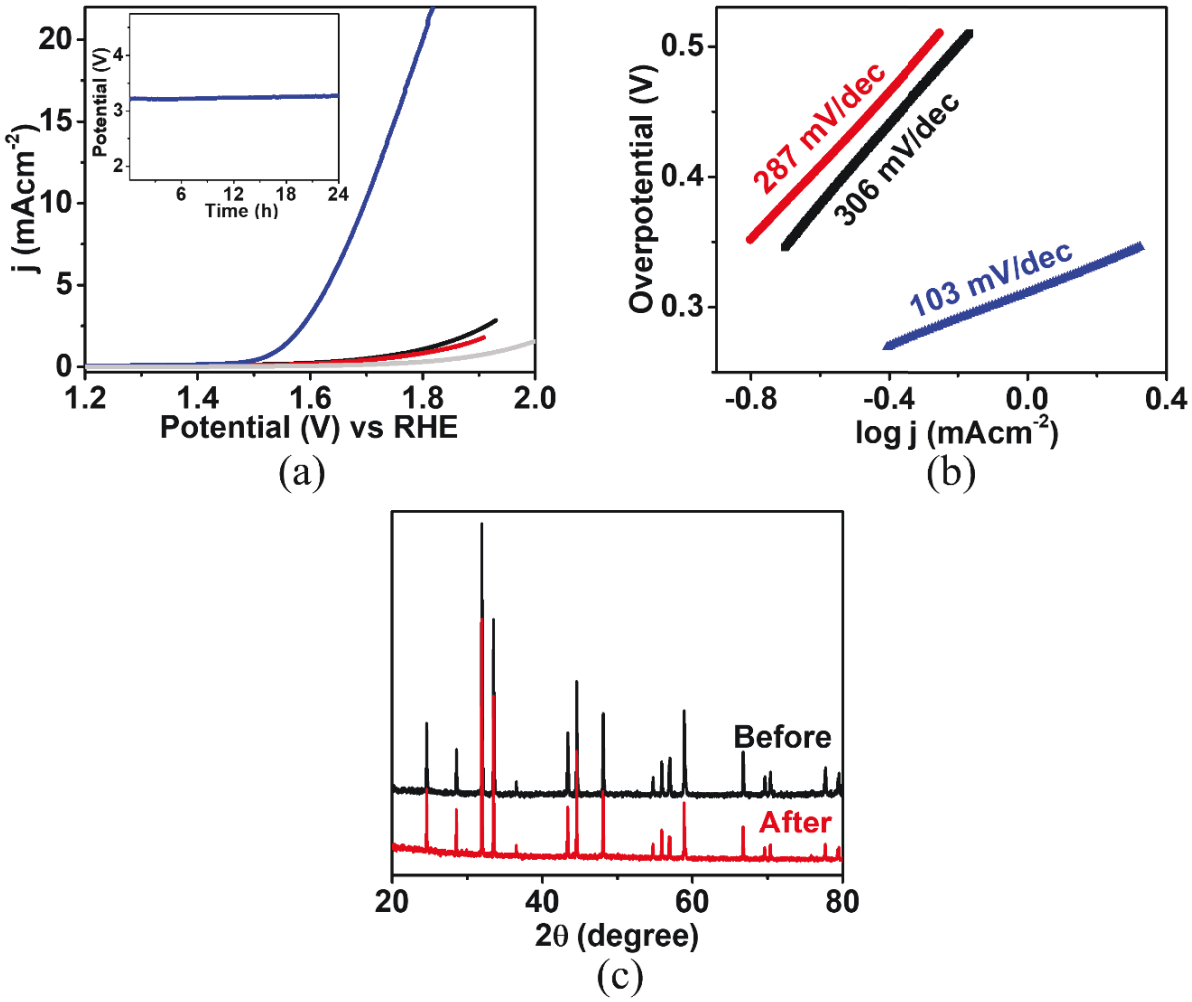


**Figure 5.** (a) Polarization curve for OER activities of $SrLaAlO_4$ (gray, impure), $SrLaAl_{1/2}Mn_{1/2}O_4$ (black), $SrLaAl_{1/2}Fe_{1/2}O_4$ (red), and $SrLaAl_{1/2}Co_{1/2}O_4$ (blue) in 0.1 M KOH. The inset shows chronopotentiometry data for the best performing catalyst, $SrLaAl_{1/2}Co_{1/2}O_4$ at 10 $mAcm^{-2}$. (b) Tafel plot and Tafel slopes for the three materials. (c) X-ray diffraction data before and after 1000 cycles of OER for $SrLaAl_{1/2}Co_{1/2}O_4$.

A more important metric to compare the catalytic activities is the overpotential (potential beyond the ideal thermodynamic potential 1.23 V) at 10 $mAcm^{-2}$, $\eta_{10}$. In this series, two materials, $SrLaAl_{1/2}Mn_{1/2}O_4$ and $SrLaAl_{1/2}Fe_{1/2}O_4$, cannot generate enough current to reach 10 $mAcm^{-2}$ in the potential window of these experiments. On the other hand, $SrLaAl_{1/2}Co_{1/2}O_4$ shows an overpotential of $\eta_{10}$ = 460 mV. The $SrLaAlO_4$ sample (impure) was also tested, showing negligible activity (grey plot in Figure 5a). A comparison of the OER activity of $SrLaAl_{1/2}Co_{1/2}O_4$ to some other materials indicates that there are other oxides such as the perovskite $CaSrFeMnO_{6-\delta}$ ($\eta_{10}$= 370 mV)[16] which have better performance. However, the activity of $SrLaAl_{1/2}Co_{1/2}O_4$ is close to that of the precious metal catalyst $IrO_2$ ($\eta_{10}$ = 400 mV).[19] Its performance is also better than several reported oxide catalysts for OER, such as BSCF ($\eta_{10}$ = 510 mV),[6] $La_{0.6}Sr_{0.4}CoO_{3-\delta}$ ($\eta_{10}$ = 590 mV),[72] $CoFe_2O_4$ nanoparticles ($\eta_{10}$ = 600 mV),[73] and $Ca_2FeMnO_{6-\delta}$ ($\eta_{10}$ = 560 mV).[16]

The evaluation of the reaction kinetics was done using the Tafel plot, $\eta$ vs log $j$. As shown in Figure 5b, $SrLaAl_{1/2}Co_{1/2}O_4$ has the smallest Tafel slope, indicating faster reaction kinetics, which is consistent with the best catalytic activity of $SrLaAl_{1/2}Co_{1/2}O_4$ in this series.

Chronopotentiometry experiment is done to study the stability of the best performing material, $SrLaAl_{1/2}Co_{1/2}O_4$, which shows a stable response for at least 24 hours, as shown in the inset of Figure 5a. X-ray diffraction data were obtained before and after OER to evaluate the structural stability of $SrLaAl_{1/2}Co_{1/2}O_4$. As shown in Figure 5c, $SrLaAl_{1/2}Co_{1/2}O_4$ retains its structural integrity after 1000 cycles of OER in basic conditions.

We have also evaluated the double layer capacitance, $C_{dl}$, which can be found from cyclic voltammograms in non-Faradaic region. In this region the current originates primarily from charge-discharge of electrical double layer, and the electrode reaction is not significant.[17, 74] The $C_{dl}$ values can be determined using the equation $C_{dl} = j_{average}/v$, where $j_{average}$ is the average of the

absolute values of $j_{anodic}$ and $j_{cathodic}$ from the CV at a specific potential and $v$ is the scan rate.[75, 76] The slope of the plot of $j_{average}$ versus $v$ gives the value of $C_{dl}$. Some researcher have used the absolute value of the difference between $j_{anodic}$ and $j_{cathodic}$, $\Delta j$, instead of $j_{average}$, and have determined $C_{dl}$ to be equal to half of the slope.[17, 58]

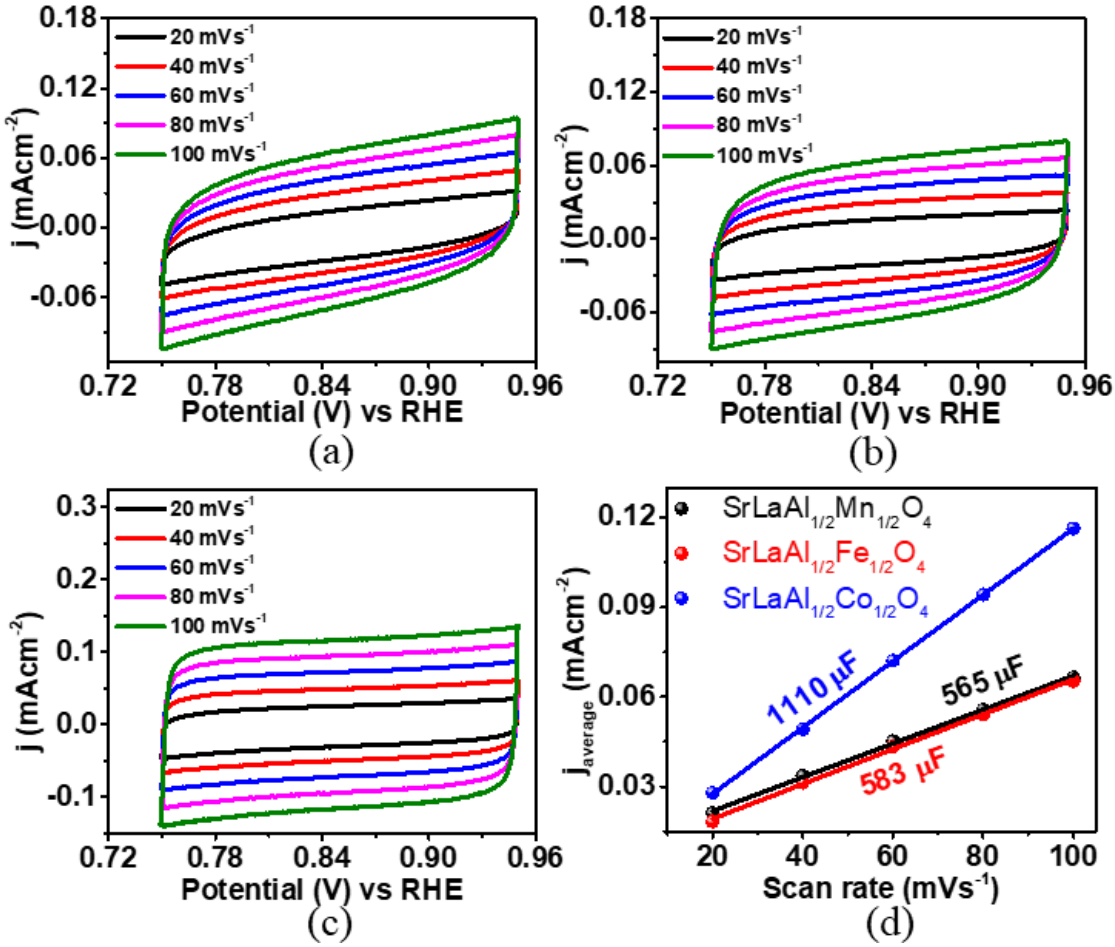


**Figure 6.** Cyclic voltammetry in the non-faradic region at different scan rates for (a) $SrLaAl_{1/2}Mn_{1/2}O_4$, (b) $SrLaAl_{1/2}Fe_{1/2}O_4$, and (c) $SrLaAl_{1/2}Co_{1/2}O_4$. Part (d) shows $j_{average}$ taken at the middle potential of 0.85 V plotted against the scan rate, where the slope gives the double layer capacitance.

In Figure 6d, the values of $j_{average}$ at the middle potential of 0.85 V are plotted against the corresponding scan rates from CVs (Figures 6a-c), and the slopes show the $C_{dl}$ values. The $C_{dl}$ of $SrLaAl_{1/2}Co_{1/2}O_4$ is almost double the values of the other two compounds. The significance of $C_{dl}$[17, 58] is its relation to the electrochemically active surface area (ECSA) through $ECSA = C_{dl}/C_s$,

where $C_s$ is specific capacitance.[17, 59, 74] $C_s$ is sometimes treated as a constant, 40 μFcm$^{-2}$, for metal electrodes.[59, 74]

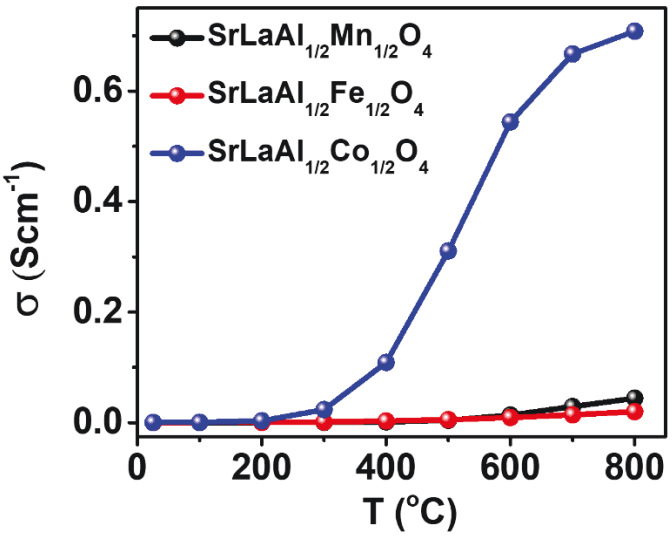


**Figure 7.** Electrical conductivity as a function of temperature.

The enhanced electrocatalytic performance of $SrLaAl_{1/2}Co_{1/2}O_4$ can be explained in terms of some previously studied descriptors for electrocatalysis,[70] including electronegativity,[77] electronic configuration[12] and electrical conductivity.[17] The greater electronegativity of Co compared to those of Mn and Fe can lead to a decrease in the metal to ligand charge transfer energy,[78] and an increase in bond covalency.[77] The enhanced covalency results in a better overlap between metal *d* and oxygen *p* orbital which can have a positive impact on the electrocatalytic activity, especially for OER.[77] This factor is combined with the effect of the electronic configuration, $d^4$ for $Mn^{3+}$, $d^5$ for $Fe^{3+}$, and $d^6$ for $Co^{3+}$. The latter has been found to be in intermediate spin state in perovskite-type oxides,[12, 79] leading to the $e_g$ orbital occupancy of 1, which has been suggested as a descriptor for the electrocatalytic performance.[12] Importantly, the results of electrical conductivity measurements (Figure 7), follow the same trend as the electrocatalytic performance. These

measurements indicate that the best catalyst in the series, $SrLaAl_{1/2}Co_{1/2}O_4$, shows a significantly higher electrical conductivity compared to the other two materials, pointing to a correlation between electrical charge transport and electrocatalytic properties.

## Conclusions

The structural and compositional flexibility makes $K_2NiF_4$-type oxides suitable candidates for electrocatalytic applications. Their functional properties can be varied by changing the B site cations. In the series $SrLaAl_{1/2}Mn_{1/2}O_4$, $SrLaAl_{1/2}Fe_{1/2}O_4$, and $SrLaAl_{1/2}Co_{1/2}O_4$, the variation of the B site cation led to a modification of the electrocatalytic properties. The latter material showed the best electrocatalytic performance toward hydrogen-evolution reaction (HER) and oxygen evolution reaction (OER), as well as enhanced reaction kinetics. The enhanced electrocatalytic activities can be attributed to a combination of factors, including the higher electronegativity of Co compared to Mn and Fe, the variation in the electronic configuration, and the electrical conductivity. The higher electronegativity of Co results in greater bond covalency and better overlap between metal 3*d* and oxygen 2*p* orbitals, which ultimately facilitates the electrocatalytic process by reducing the charge transfer resistance. In addition, the electronic configuration of trivalent cobalt leads to an $e_g$ occupancy of 1. This factor, combined with the higher electrical conductivity of $SrLaAl_{1/2}Co_{1/2}O_4$, reinforces the impact of the electronegativity, leading to the enhanced electrocatalytic performance of this material.

**Acknowledgement.** This work is supported by the National Science Foundation (NSF) under grant no. DMR-1943085.

**References**


1. Yang, Z.; Zhang, J.; Kintner-Meyer, M. C. W.; Lu, X.; Choi, D.; Lemmon, J. P.; Liu, J., Electrochemical Energy Storage for Green Grid. *Chem. Rev.* **2011,** *111* (5), 3577-3613.
2. Lewis, N. S.; Nocera, D. G., Powering the planet: Chemical challenges in solar energy utilization. *Proc. of the Natl. Acad. Sci.* **2006,** *103* (43), 15729.
3. Badreldin, A.; Abusrafa, A. E.; Abdel-Wahab, A., Oxygen-Deficient Cobalt-Based Oxides for Electrocatalytic Water Splitting. *ChemSusChem* **2021,** *14* (1), 10-32.
4. Hu, C.; Zhang, L.; Gong, J., Recent progress made in the mechanism comprehension and design of electrocatalysts for alkaline water splitting. *Energy Environ. Sci.* **2019,** *12* (9), 2620-2645.
5. Joo, J.; Kim, T.; Lee, J.; Choi, S.-I.; Lee, K., Morphology-Controlled Metal Sulfides and Phosphides for Electrochemical Water Splitting. *Adv. Mater.* **2019,** *31* (14), 1806682.
6. Zhu, Y.; Zhou, W.; Chen, Z.-G.; Chen, Y.; Su, C.; Tadé, M. O.; Shao, Z., $SrNb_{0.1}Co_{0.7}Fe_{0.2}O_{3-\delta}$ Perovskite as a Next-Generation Electrocatalyst for Oxygen Evolution in Alkaline Solution. *Angew. Chem. Int. Ed.* **2015,** *54* (13), 3897-3901.
7. Das, D.; Das, A.; Reghunath, M.; Nanda, K. K., Phosphine-free avenue to $Co_2P$ nanoparticle encapsulated N,P co-doped CNTs: a novel non-enzymatic glucose sensor and an efficient electrocatalyst for oxygen evolution reaction. *Green Chem.* **2017,** *19* (5), 1327-1335.
8. Xu, X.; Chen, Y.; Zhou, W.; Zhu, Z.; Su, C.; Liu, M.; Shao, Z., A Perovskite Electrocatalyst for Efficient Hydrogen Evolution Reaction. *Adv. Mater.* **2016,** *28* (30), 6442-6448.
9. Zhu, Y.; Zhou, W.; Zhong, Y.; Bu, Y.; Chen, X.; Zhong, Q.; Liu, M.; Shao, Z., A Perovskite Nanorod as Bifunctional Electrocatalyst for Overall Water Splitting. *Adv. Energy Mater.* **2017,** *7* (8), 1602122.
10. Septiani, N. L. W.; Kaneti, Y. V.; Fathoni, K. B.; Kani, K.; Allah, A. E.; Yuliarto, B.; Nugraha; Dipojono, H. K.; Alothman, Z. A.; Golberg, D.; Yamauchi, Y., Self-Assembly of Two-Dimensional Bimetallic Nickel–Cobalt Phosphate Nanoplates into One-Dimensional Porous Chainlike Architecture for Efficient Oxygen Evolution Reaction. *Chem. Mater.* **2020,** *32* (16), 7005-7018.
11. Septiani, N. L. W.; Kaneti, Y. V.; Guo, Y.; Yuliarto, B.; Jiang, X.; Ide, Y.; Nugraha, N.; Dipojono, H. K.; Yu, A.; Sugahara, Y.; Golberg, D.; Yamauchi, Y., Holey Assembly of Two-Dimensional Iron-Doped Nickel-Cobalt Layered Double Hydroxide Nanosheets for Energy Conversion Application. *ChemSusChem* **2020,** *13* (6), 1645-1655.
12. Suntivich, J.; May, K. J.; Gasteiger, H. A.; Goodenough, J. B.; Shao-Horn, Y., A Perovskite Oxide Optimized for Oxygen Evolution Catalysis from Molecular Orbital Principles. *Science* **2011,** *334* (6061), 1383.
13. Karki, S. B.; Andriotis, A. N.; Menon, M.; Ramezanipour, F., Bifunctional Water-Splitting Electrocatalysis Achieved by Defect Order in $LaA_2Fe_3O_8$ (A = Ca, Sr). *ACS Appl. Energy Mater.* **2021,** *4* (11), 12063-12066.
14. Hona, R. K.; Karki, S. B.; Cao, T.; Mishra, R.; Sterbinsky, G. E.; Ramezanipour, F., Sustainable Oxide Electrocatalyst for Hydrogen- and Oxygen-Evolution Reactions. *ACS Catal.* **2021**, 14605-14614.
15. Karki, S. B.; Ramezanipour, F., Pseudocapacitive Energy Storage and Electrocatalytic Hydrogen-Evolution Activity of Defect-Ordered Perovskites $Sr_xCa_{3-x}GaMn_2O_8$ (x = 0 and 1). *ACS Appl. Energy Mater.* **2020,** *3* (11), 10983-10992.
16. Hona, R. K.; Karki, S. B.; Ramezanipour, F., Oxide Electrocatalysts Based on Earth-Abundant Metals for Both Hydrogen- and Oxygen-Evolution Reactions. *ACS Sustainable Chem. Eng.* **2020,** *8* (31), 11549-11557.
17. Hona, R. K.; Ramezanipour, F., Remarkable Oxygen-Evolution Activity of a Perovskite Oxide from the $Ca_{2-x}Sr_xFe_2O_{6-\delta}$ Series. *Angew. Chem. Int. Ed.* **2019,** *58* (7), 2060-2063.
18. Alom, M. S.; Ramezanipour, F., Layered Oxides $SrLaFe_{1-x}Co_xO_{4-\delta}$ (x=0–1) as Bifunctional Electrocatalysts for Water-Splitting. *ChemCatChem* **2021,** *13* (15), 3510-3516.
19. Kananke-Gamage, C. C. W.; Ramezanipour, F., Variation of the electrocatalytic activity of isostructural oxides $Sr_2LaFeMnO_7$ and $Sr_2LaCoMnO_7$ for hydrogen and oxygen-evolution reactions. *Dalton Trans.* **2021,** *50* (40), 14196-14206.

20. Karki, S. B.; Hona, R. K.; Yu, M.; Ramezanipour, F., Enhancement of Electrocatalytic Activity as a Function of Structural Order in Perovskite Oxides. *ACS Catal.* **2022,** *12*, 10333-10337.
21. Xu, L.; Yin, Y.-M.; Zhou, N.; Wang, Z.; Ma, Z.-F., Sulfur tolerant redox stable layered perovskite $SrLaFeO_{4-\delta}$ as anode for solid oxide fuel cells. *Electrochem. Commun.* **2017,** *76*, 51-54.
22. Kharton, V. V.; Yaremchenko, A. A.; Shaula, A. L.; Patrakeev, M. V.; Naumovich, E. N.; Logvinovich, D. I.; Frade, J. R.; Marques, F. M. B., Transport properties and stability of Ni-containing mixed conductors with perovskite- and $K_2NiF_4$-type structure. *J. Solid State Chem.* **2004,** *177* (1), 26-37.
23. Wu, N.; Wang, W.; Zhong, Y.; Yang, G.; Qu, J.; Shao, Z., Nickel-Iron Alloy Nanoparticle-Decorated $K_2NiF_4$-Type Oxide as an Efficient and Sulfur-Tolerant Anode for Solid Oxide Fuel Cells. *ChemElectroChem* **2017,** *4* (9), 2378-2384.
24. Soderholm, L.; Williams, C. W.; Welp, U., The superconductor-related oxides $Cm_2CuO_4$ and $Cm_{1.83}Th_{0.17}CuO_4$. *Physica C Supercond.* **1991,** *179* (4), 440-446.
25. Chu, C. W.; Hor, P. H.; Meng, R. L.; Gao, L.; Huang, Z. J., Superconductivity at 52.5 K in the Lanthanum-Barium-Copper-Oxide System. *Science* **1987,** *235* (4788), 567.
26. Wang, X. L.; Takayama-Muromachi, E., Magnetic and transport properties of the layered perovskite system $Sr_{2-y}Y_yCoO_4$ ($0 \leqslant y \leqslant 1$). *Phys. Rev. B* **2005,** *72* (6), 064401.
27. Wang, X. L.; Takayama-Muromachi, E.; Dou, S. X.; Cheng, Z. X., Band structures, magnetic properties, and enhanced magnetoresistance in the high pressure phase of Gd and Y doped two-dimensional perovskite $Sr_2CoO_4$ compounds. *Appl. Phys. Lett.* **2007,** *91* (6), 062501.
28. Arbuckle, B. W.; Ramanujachary, K. V.; Zhang, Z.; Greenblatt, M., Investigations on the structural, electrical, and magnetic properties of $Nd_{2-x}Sr_xNiO_{4+\delta}$. *J. Solid State Chem.* **1990,** *88* (1), 278-290.
29. Arbuckle, B. W.; Ramanujachary, K. V.; Buckley, A. M.; Greenblatt, M., Preparation and investigation of the physical properties of fluorinated $Nd_{2-x}Sr_xNiO_{4+\delta}$. *J. Solid State Chem.* **1992,** *97* (2), 274-282.
30. Alom, M. S.; Ramezanipour, F., Pseudocapacitive charge storage in layered oxides $SrLaFe_{1-x}Co_xO_{4-\delta}$ (x = 0–1). *Mater. Lett.* **2021,** *295*, 129859.
31. Zhu, Y.; Tahini, H. A.; Hu, Z.; Dai, J.; Chen, Y.; Sun, H.; Zhou, W.; Liu, M.; Smith, S. C.; Wang, H.; Shao, Z., Unusual synergistic effect in layered Ruddlesden−Popper oxide enables ultrafast hydrogen evolution. *Nat. Commun.* **2019,** *10* (1), 149.
32. Yin, B.; Li, Y.; Sun, N.; Ji, X.; Huan, Y.; Dong, D.; Hu, X.; Wei, T., Activating ORR and OER in Ruddlesden-Popper based catalysts by enhancing interstitial oxygen and lattice oxygen redox reactions. *Electrochim. Acta* **2021,** *370*, 137747.
33. Demazeau, G.; Byeon, S. H.; Hagenmuller, P.; Choy, J. H., Influence des Liaisons Chimiques sur la Transition Spin Faible → Spin Fort du Cobalt(III) ($3d^6$) au sein D′Oxydes de Type $K_2NiF_4$. *Z. anorg. allg. Chem.* **1992,** *610* (4), 91-98.
34. Larson, A. C.; Dreele, R. B., General structure analysis system (GSAS). *Los Alamos National Laboratory Report LAUR* **1994**, 86-748.
35. Toby, B., EXPGUI, a graphical user interface for GSAS. *J. Appl. Crystallogr.* **2001,** *34*, 210-213.
36. Hona, R. K.; Ramezanipour, F., Effect of the Oxygen Vacancies and Structural Order on the Oxygen Evolution Activity: A Case Study of $SrMnO_{3-\delta}$ Featuring Four Different Structure Types. *Inorg. Chem.* **2020,** *59* (7), 4685-4692.
37. Karki, S. B.; Hona, R. K.; Ramezanipour, F., Electrocatalytic activity and structural transformation of $Ca_2Sr_2Mn_2MO_{10-\delta}$ (M = Fe, Co). *Ionics* **2022,** *28* (1), 397-406.
38. Wei, C.; Rao, R. R.; Peng, J.; Huang, B.; Stephens, I. E. L.; Risch, M.; Xu, Z. J.; Shao-Horn, Y., Recommended Practices and Benchmark Activity for Hydrogen and Oxygen Electrocatalysis in Water Splitting and Fuel Cells. *Adv. Mater.* **2019,** *31* (31), 1806296.
39. Jin, C.; Cao, X.; Zhang, L.; Zhang, C.; Yang, R., Preparation and electrochemical properties of urchin-like $La_{0.8}Sr_{0.2}MnO_3$ perovskite oxide as a bifunctional catalyst for oxygen reduction and oxygen evolution reaction. *J. Power Sources* **2013,** *241*, 225-230.

40. May, K. J.; Carlton, C. E.; Stoerzinger, K. A.; Risch, M.; Suntivich, J.; Lee, Y.-L.; Grimaud, A.; Shao-Horn, Y., Influence of Oxygen Evolution during Water Oxidation on the Surface of Perovskite Oxide Catalysts. *J. Phys. Chem. Lett.* **2012,** *3* (22), 3264-3270.
41. Malkhandi, S.; Trinh, P.; Manohar, A. K.; Jayachandrababu, K. C.; Kindler, A.; Surya Prakash, G. K.; Narayanan, S. R., Electrocatalytic Activity of Transition Metal Oxide-Carbon Composites for Oxygen Reduction in Alkaline Batteries and Fuel Cells. *J. Electrochem. Soc.* **2013,** *160* (9), F943-F952.
42. Goldschmidt, V. M., Die Gesetze der Krystallochemie. *Naturwissenschaften* **1926,** *14* (21), 477-485.
43. Nirala, G.; Yadav, D.; Upadhyay, S., Ruddlesden-Popper phase $A_2BO_4$ oxides: Recent studies on structure, electrical, dielectric, and optical properties. *J. Adv. Ceram.* **2020,** *9* (2), 129-148.
44. Wilhelm, H.; Cros, C.; Reny, E.; Demazeau, G.; Hanfland, M., Pressure-Induced Structural Phase Transitions in $Ln_{2-x}Nd_xCuO_4$ for Ln=La ($0.6\leq x\leq 2$) and Ln=Pr (x=0). *J. Solid State Chem.* **2000,** *151* (2), 231-240.
45. Singh, D.; Singh, S.; Mahajan, A.; Choudhary, N., Effect of substitution of magnetic rare earth Nd at non-magnetic La site on structure and properties of $LaSrFeO_4$. *Ceram. Int.* **2014,** *40* (1, Part A), 1183-1188.
46. Sanson, A.; Kantor, I.; Cerantola, V.; Irifune, T.; Carnera, A.; Pascarelli, S., Local structure and spin transition in $Fe_2O_3$ hematite at high pressure. *Phys. Rev. B* **2016,** *94*, 014112.
47. Shannon, R. D., Revised effective ionic radii and systematic studies of interatomic distances in halides and chalcogenides. *Acta Cryst. A* **1976,** *32* (5), 751-767.
48. Hona, R. K.; Huq, A.; Ramezanipour, F., Unraveling the Role of Structural Order in the Transformation of Electrical Conductivity in $Ca_2FeCoO_{6-\delta}$, $CaSrFeCoO_{6-\delta}$, and $Sr_2FeCoO_{6-\delta}$. *Inorg. Chem.* **2017,** *56*, 14494-14505.
49. Conway, B. E.; Tilak, B. V., Interfacial processes involving electrocatalytic evolution and oxidation of $H_2$, and the role of chemisorbed H. *Electrochim. Acta* **2002,** *47* (22), 3571-3594.
50. Xiao, X.; Engelbrekt, C.; Li, Z.; Si, P., Hydrogen evolution at nanoporous gold/tungsten sulfide composite film and its optimization. *Electrochim. Acta* **2015,** *173*, 393-398.
51. Alom, M. S.; Kananke-Gamage, C. C. W.; Ramezanipour, F., Perovskite Oxides as Electrocatalysts for Hydrogen Evolution Reaction. *ACS Omega* **2022,** *7* (9), 7444-7451.
52. Anantharaj, S.; Ede, S. R.; Sakthikumar, K.; Karthick, K.; Mishra, S.; Kundu, S., Recent Trends and Perspectives in Electrochemical Water Splitting with an Emphasis on Sulfide, Selenide, and Phosphide Catalysts of Fe, Co, and Ni: A Review. *ACS Catal.* **2016,** *6* (12), 8069-8097.
53. Zhang, L.-N.; Li, S.-H.; Tan, H.-Q.; Khan, S. U.; Ma, Y.-Y.; Zang, H.-Y.; Wang, Y.-H.; Li, Y.-G., MoP/$Mo_2C$@C: A New Combination of Electrocatalysts for Highly Efficient Hydrogen Evolution over the Entire pH Range. *ACS Appl. Mater. Interfaces* **2017,** *9* (19), 16270-16279.
54. Wu, C.; Liu, D.; Li, H.; Li, J., Molybdenum Carbide-Decorated Metallic Cobalt@Nitrogen-Doped Carbon Polyhedrons for Enhanced Electrocatalytic Hydrogen Evolution. *Small* **2018,** *14* (16), 1704227.
55. Cao, J.; Zhou, J.; Zhang, Y.; Zou, Y.; Liu, X., $MoS_2$ nanosheets direct supported on reduced graphene oxide: An advanced electrocatalyst for hydrogen evolution reaction. *PLOS ONE* **2017,** *12* (5), e0177258.
56. Li, Y. H.; Liu, P. F.; Pan, L. F.; Wang, H. F.; Yang, Z. Z.; Zheng, L. R.; Hu, P.; Zhao, H. J.; Gu, L.; Yang, H. G., Local atomic structure modulations activate metal oxide as electrocatalyst for hydrogen evolution in acidic water. *Nat. Commun.* **2015,** *6* (1), 8064.
57. Galal, A.; Hassan, H. K.; Atta, N. F.; Jacob, T., An Efficient and Durable Electrocatalyst for Hydrogen Production Based on Earth-Abundant Oxide-Graphene Composite. *ChemistrySelect* **2017,** *2* (31), 10261-10270.
58. Pan, Y.; Chen, Y.; Li, X.; Liu, Y.; Liu, C., Nanostructured nickel sulfides: phase evolution, characterization and electrocatalytic properties for the hydrogen evolution reaction. *RSC Adv.* **2015,** *5* (127), 104740-104749.

59. Oh, S.; Kim, H.; Kwon, Y.; Kim, M.; Cho, E.; Kwon, H., Porous Co–P foam as an efficient bifunctional electrocatalyst for hydrogen and oxygen evolution reactions. *J. Mater. Chem. A* **2016,** *4* (47), 18272-18277.
60. Song, F.; Hu, X., Ultrathin Cobalt–Manganese Layered Double Hydroxide Is an Efficient Oxygen Evolution Catalyst. *J. Am. Chem. Soc.* **2014,** *136* (47), 16481-16484.
61. Moir, J.; Soheilnia, N.; O'Brien, P.; Jelle, A.; Grozea, C. M.; Faulkner, D.; Helander, M. G.; Ozin, G. A., Enhanced Hematite Water Electrolysis Using a 3D Antimony-Doped Tin Oxide Electrode. *ACS Nano* **2013,** *7* (5), 4261-4274.
62. Zou, X.; Zhang, Y., Noble metal-free hydrogen evolution catalysts for water splitting. *Chem. Soc. Rev.* **2015,** *44* (15), 5148-5180.
63. Chaitoglou, S.; Giannakopoulou, T.; Speliotis, T.; Vavouliotis, A.; Trapalis, C.; Dimoulas, A., $Mo_2C$/graphene heterostructures: low temperature chemical vapor deposition on liquid bimetallic Sn-Cu and hydrogen evolution reaction electrocatalytic properties. *Nanotechnology* **2019,** *30* (12), 125401.
64. Liu, M.-R.; Hong, Q.-L.; Li, Q.-H.; Du, Y.; Zhang, H.-X.; Chen, S.; Zhou, T.; Zhang, J., Cobalt Boron Imidazolate Framework Derived Cobalt Nanoparticles Encapsulated in B/N Codoped Nanocarbon as Efficient Bifunctional Electrocatalysts for Overall Water Splitting. *Adv. Func. Mater.* **2018,** *28* (26), 1801136.
65. Xi, W.; Yan, G.; Tan, H.; Xiao, L.; Cheng, S.; Khan, S. U.; Wang, Y.; Li, Y., Superaerophobic P-doped $Ni(OH)_2/NiMoO_4$ hierarchical nanosheet arrays grown on Ni foam for electrocatalytic overall water splitting. *Dalton Trans.* **2018,** *47* (26), 8787-8793.
66. Zhang, X.; Zhang, M.; Tian, Y.; You, J.; Yang, C.; Su, J.; Li, Y.; Gao, Y.; Gu, H., In situ synthesis of $MoS_2$/graphene nanosheets as free-standing and flexible electrode paper for high-efficiency hydrogen evolution reaction. *RSC Adv.* **2018,** *8* (19), 10698-10705.
67. Lai, B.; Singh, S. C.; Bindra, J. K.; Saraj, C. S.; Shukla, A.; Yadav, T. P.; Wu, W.; McGill, S. A.; Dalal, N. S.; Srivastava, A.; Guo, C., Hydrogen evolution reaction from bare and surface-functionalized few-layered $MoS_2$ nanosheets in acidic and alkaline electrolytes. *Mater. Today Chem.* **2019,** *14*, 100207.
68. Suen, N.-T.; Hung, S.-F.; Quan, Q.; Zhang, N.; Xu, Y.-J.; Chen, H. M., Electrocatalysis for the oxygen evolution reaction: recent development and future perspectives. *Chem. Soc. Rev.* **2017,** *46* (2), 337-365.
69. Dau, H.; Limberg, C.; Reier, T.; Risch, M.; Roggan, S.; Strasser, P., The Mechanism of Water Oxidation: From Electrolysis via Homogeneous to Biological Catalysis. *ChemCatChem* **2010,** *2* (7), 724-761.
70. Song, F.; Bai, L.; Moysiadou, A.; Lee, S.; Hu, C.; Liardet, L.; Hu, X., Transition Metal Oxides as Electrocatalysts for the Oxygen Evolution Reaction in Alkaline Solutions: An Application-Inspired Renaissance. *J. Am. Chem. Soc.* **2018,** *140* (25), 7748-7759.
71. Benck, J. D.; Hellstern, T. R.; Kibsgaard, J.; Chakthranont, P.; Jaramillo, T. F., Catalyzing the Hydrogen Evolution Reaction (HER) with Molybdenum Sulfide Nanomaterials. *ACS Catal.* **2014,** *4* (11), 3957-3971.
72. Oh, M. Y.; Jeon, J. S.; Lee, J. J.; Kim, P.; Nahm, K. S., The bifunctional electrocatalytic activity of perovskite $La_{0.6}Sr_{0.4}CoO_{3-\delta}$ for oxygen reduction and evolution reactions. *RSC Adv.* **2015,** *5* (25), 19190-19198.
73. Li, M.; Xiong, Y.; Liu, X.; Bo, X.; Zhang, Y.; Han, C.; Guo, L., Facile synthesis of electrospun $MFe_2O_4$ (M = Co, Ni, Cu, Mn) spinel nanofibers with excellent electrocatalytic properties for oxygen evolution and hydrogen peroxide reduction. *Nanoscale* **2015,** *7* (19), 8920-8930.
74. Jung, S.; McCrory, C. C. L.; Ferrer, I. M.; Peters, J. C.; Jaramillo, T. F., Benchmarking nanoparticulate metal oxide electrocatalysts for the alkaline water oxidation reaction. *J. Mater. Chem. A* **2016,** *4* (8), 3068-3076.
75. Zhu, Y.; Zhou, W.; Sunarso, J.; Zhong, Y.; Shao, Z., Phosphorus-Doped Perovskite Oxide as Highly Efficient Water Oxidation Electrocatalyst in Alkaline Solution. *Adv. Func. Mater.* **2016,** *26* (32), 5862-5872.

76. Petrie, J. R.; Cooper, V. R.; Freeland, J. W.; Meyer, T. L.; Zhang, Z.; Lutterman, D. A.; Lee, H. N., Enhanced Bifunctional Oxygen Catalysis in Strained $LaNiO_3$ Perovskites. *J. Am. Chem. Soc.* **2016,** *138* (8), 2488-2491.
77. Suntivich, J.; Hong, W. T.; Lee, Y.-L.; Rondinelli, J. M.; Yang, W.; Goodenough, J. B.; Dabrowski, B.; Freeland, J. W.; Shao-Horn, Y., Estimating Hybridization of Transition Metal and Oxygen States in Perovskites from O K-edge X-ray Absorption Spectroscopy. *J. Phys. Chem. C* **2014,** *118* (4), 1856-1863.
78. Saitoh, T.; Bocquet, A. E.; Mizokawa, T.; Fujimori, A., Systematic variation of the electronic structure of 3d transition-metal compounds. *Phys. Rev. B* **1995,** *52* (11), 7934-7938.
79. Moritomo, Y.; Higashi, K.; Matsuda, K.; Nakamura, A., Spin-state transition in layered perovskite cobalt oxides: $La_{2-x}Sr_xCoO_4$ ($0.4 \leq x \leq 1.0$). *Phys. Rev. B* **1997,** *55* (22), R14725-R14728.